I. FORMALISM OF NON-STANDARD INTERACTIONS

Non-standard interactions are sub-leading contributions to neutrino flavor transitions arising from neutrino interactions not considered in the Standard Model. We consider matter NSIs arising from the neutral current NSIs, which exclude production and detection effects. An effective four-fermion Lagrangian for this type of interaction can be written as

$$\mathcal{L}_{\text{NC}} = -2\sqrt{2}G_F\epsilon_{\alpha\beta}^{fX} \left(\bar{\nu}_\alpha\gamma^\mu P_L\nu_\beta\right)\left(\bar{f}\gamma_\mu P_X f\right) , \tag{1}$$

where NC denotes the neutral current interaction with $f \in \{e, u, d\}$, and P_X is the chirality projection operators with $X \in \{L, R\}$.

For chirality X, the NSI Hamiltonian takes the form

$$H = \frac{1}{2E}UM^2U^\dagger + \sqrt{2}G_F n_e\text{diag}(1,0,0) + \sqrt{2}G_F\sum_f n_f\epsilon^{fX} \tag{2}$$

We have no independent sensitivity for the chirality of ϵ^{fX}, so we sum over these to obtain the vectorial parameter as $\epsilon_{\alpha\beta}^{fV} = \epsilon_{\alpha\beta}^{fL} + \epsilon_{\alpha\beta}^{fR}$. Moreover, we normalize the fermion number density n_f by the electron number density n_e. Our matter study will be wholly confined to the interior of the Earth, where we assume electrical neutrality and equal distribution of neutrons and protons, so we use the relations $n_u/n_e \simeq n_d/n_e \simeq 3$. The effective NSI parameters in matter now take the form

$$\begin{aligned}\epsilon_{\alpha\beta} &= \sum_{f,X}\frac{n_f}{n_e}\epsilon_{\alpha\beta}^{fX} \\ &= \epsilon_{\alpha\beta}^{eV} + 3\,\epsilon_{\alpha\beta}^{uV} + 3\,\epsilon_{\alpha\beta}^{dV}\end{aligned} \tag{3}$$

We note that our definition of $\epsilon_{\alpha\beta}$ differs from e.g. [1], where the quark number density is used to normalize the parameters.

With the matter potential $V = \sqrt{2}G_F n_e$, we write

$$H = \frac{1}{2E}UM^2U^\dagger + V\begin{bmatrix}1+\epsilon_{ee} & \epsilon_{e\mu} & \epsilon_{e\tau} \\ \epsilon_{e\mu} & \epsilon_{\mu\mu} & \epsilon_{\mu\tau} \\ \epsilon_{e\tau} & \epsilon_{\mu\tau} & \epsilon_{\tau\tau}\end{bmatrix} , \tag{4}$$

where we have assumed the components of the NSI matrix to be real.

To propagate the neutrino states through the Earth, we solve the Schrödinger equation with the Hamiltonian from Eq. 4. The Earth density profile is taken from the PREM [2], and we do not consider neutrino absorption. The baseline for a given trajectory is determined using an average neutrino production height of 15 km and an Earth radius of 6371 km. Thus, matter oscillations introduce a zenith angle dependence in two areas. Firstly, the matter potential depends on the matter density through the neutrino propagates. A neutrino with $\cos\theta_z < -0.87$ will traverse through the dense Earth core, whereas a mantle-crossing neutrino with $\cos\theta_z > -0.87$ will not. Secondly, the zenith angle also alters the baseline through which a neutrino undergoes matter oscillations. After this, we are ready to study the NSI effect on probability level.

A. NSI phenomenology at probability level

Since neutrinos and antineutrinos have different cross sections, they are treated separately in the detector simulations. However, for the purpose of qualitatively elucidating the NSI effect in this subsection, we take the effective area of ν_μ and $\bar{\nu}_\mu$ to be equal. Thus, we simply add the neutrino to the antineutrino contributions in both Fig. 1 and Fig. 2.

In the $\mu\tau$ sector, we have a resonance in the $20\,\text{GeV}$ region. Any NSI parameter involving the μ or τ channel will dampen this resonance, with some also shifting the probability in the stationary region above $100\,\text{GeV}$. This 'double effect' of both resonance dampening and shifting happens in two cases: either when the NSI parameter shares one channel with a survival probability (e.g. $\epsilon_{e\mu}$ and $P_{\mu\mu}$), or when the sectors align (e.g. $\epsilon_{\mu\tau}$ and $P_{\mu\tau}$). The only exception to this is for $P_{\tau\tau}$, which due to the near-maximal mixing in the $\mu\tau$ sector displays dampening for $\epsilon_{e\mu}$ even though they share no channel directly. We illustrate the three different effects in Fig. 1.

Due to the lightness of Δm_{21}^2, the e channel has no resonance in the GeV range. Thus, the only impact that the NSI parameters considered here can have on any ν_e probability is shifting, and this only occurs when the requirements
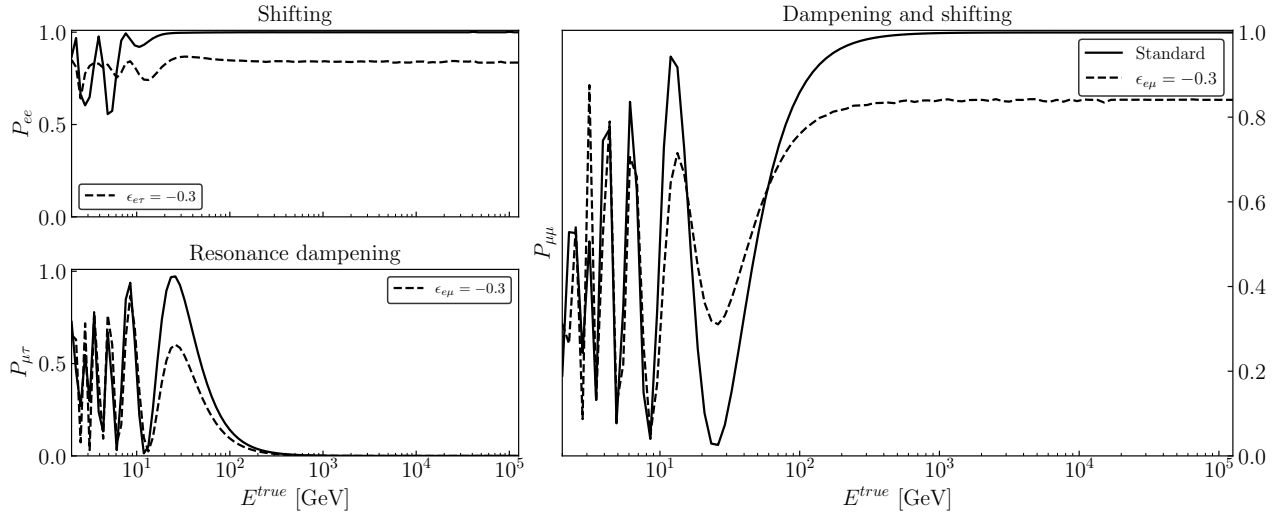
FIG. 1: The three different effects that the off-diagonal NSI parameters have in the GeV range. To schematically elucidate the NSI effect, we plot the summed probabilities for both neutrinos and antineutrinos.

for the 'double effect' are met. So except for the survival probability P_{ee}, any NSI parameter whose sector does not match the probability sector will not drastically affect it. Thus, the only off-diagonal NSI parameters that strongly affect the transition probabilities $P_{\alpha\beta}$ are $\epsilon_{\gamma\beta}$, while the survival probabilities $P_{\alpha\alpha}$ are only strongly affected by $\epsilon_{\alpha\beta}$.

B. NSI phenomenology at flux level

To study the NSI flux effect, we propagate the atmospheric neutrino flux from Honda et al [3] through the Earth. The oscillation probability $P_{\alpha\beta}$ acts as a weight to the atmospheric flux, yielding the propagated flux for flavor β at detector level as

$$\phi_\beta^{\mathrm{det}} = \sum_\alpha P_{\alpha\beta} \phi_\alpha^{\mathrm{atm}}, \tag{5}$$

where we sum over the initial lepton flavors $\alpha \in \{e, \mu, \bar{e}, \bar{\mu}\}$. To illustrate the impact of $\epsilon_{\mu\tau}$ at flux level, we plot in Fig. 2 the quantity $(\phi_{\nu_\mu}^{NSI} + \phi_{\bar{\nu}_\mu}^{NSI})/(\phi_{\nu_\mu}^{SI} + \phi_{\bar{\nu}_\mu}^{SI})$, where all fluxes are propagated to detector level by Eq. 5. In the left (right) panel, we plot the flux in region in which 99% of the DeepCore (IceCube) track events originating from $\nu_\mu + \bar{\nu}_\mu$ fluxes are contained. We see that the only clear signal discernible to the IceCube detector is a energy-independent flux deficiency with a factor in the order of $\sim 10^{0.5}$ from core-crossing neutrinos within a zenith range of $\cos\left(\theta_z^T\right) < -0.87$. DeepCore on the other hand, is exposed to multiple fringes of flux surpluses with a factor in the order of ~ 10. The strongest surplus at 20 GeV is very weakly zenith dependent, a stark contrast to the energy-independent but zenith-sensitive IceCube deficiency.

The muonic flux not only carries the largest $\epsilon_{\mu\tau}$ effect, but it is also more abundant than the ν_e flux. Thus, we expect to receive the highest statistics from μ-related NSI parameters, thus constraining them the strongest. $\epsilon_{\alpha\beta}$ which are only indirectly weakly dependent on the μ channel will have the weakest bounds. This could be improved by considering cascade events in IceCube, thus opening up the e and τ channels there.

II. DETECTOR FORMALISM

The IceCube Neutrino Observatory is a gigaton Cherenkov detector located within Antarctic ice near the Geographic South Pole. It consists of 5160 individual digital optical modules situated on 86 strings, which detect Cherenkov light emitted by charged leptons from neutrino events. We distinguish between two interaction topologies: track- and cascade-like events. Track-like events originate mainly from muons originating from ν_μ CC interactions, while cascades predominantly consist of electromagnetic and hadronic showers.
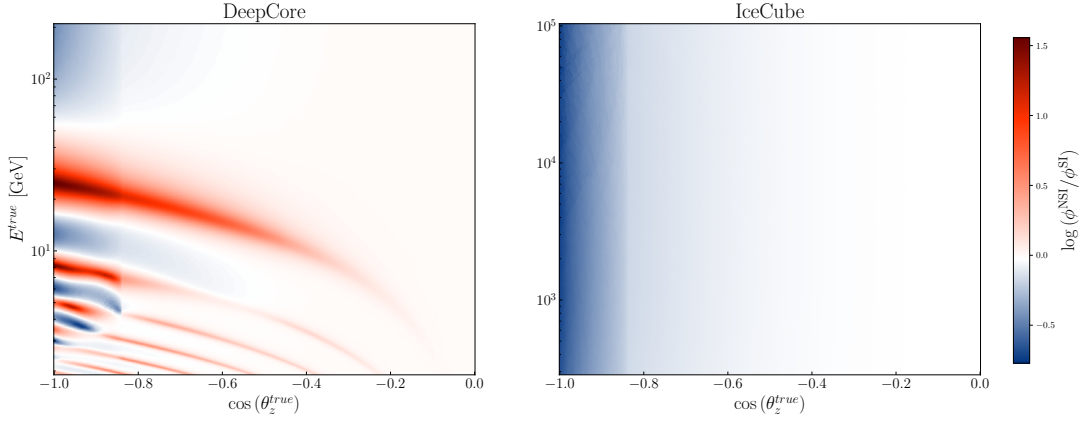
FIG. 2: Ratio of detector NSI to SI atmospheric $\nu_\mu + \bar{\nu}_\mu$ fluxes expressed as $(\phi_{\nu_\mu}^{NSI} + \phi_{\bar{\nu}_\mu}^{NSI})/(\phi_{\nu_\mu}^{SI} + \phi_{\bar{\nu}_\mu}^{SI})$. We set $\epsilon_{\mu\tau} = -0.05$, and all other $\epsilon_{\alpha\beta} = 0$. Left (right) panel shows the flux ratio in the energy range in which 99% of the simulated DeepCore (IceCube) events are contained.

DeepCore is a dense sub-array whithin the standard IceCube array, which allows us to observe neutrino interactions down to a few GeV [4]. Due to its lower energy threshold compared with IceCube, DeepCore has previously been used to study NSI effects in this more discernible range[1, 4].

PINGU is a proposed 26 string in-fill array to IceCube, consisting of optical modules of similar nature [5]. While porposed to mainly shed light on neutrino mass ordering, PINGU will be able to probe NSI parameters aswell.

A. IceCube

We obtain the data from the IC-86 sterile data release [6], which contain muon track events collected over 8 years. In the data, the reconstructed energy E^R is logarithmically binned between $500\,\text{GeV}$ to $9976\,\text{GeV}$, totalling 13 bins (index i). The reconstructed cosine-zenith $\cos(\theta_z^R)$ is linearly binned between -1 and 0 in 20 bins (index j).

The event count for each bin reads

$$N_{ij} = T \sum_\beta \int_{(\cos(\theta_z^R))_j}^{(\cos(\theta_z^R))_{j+1}} \mathrm{d}\cos(\theta_z^R) \int_{E_i^R}^{E_{i+1}^R} \mathrm{d}E^R \int_0^\pi R(\theta^R, \theta^T)\mathrm{d}\cos(\theta_z^T) \int_0^\infty \phi_\beta^{\text{det}}(E^T, \theta^R)A^{\text{eff}}(E^T)R(E^R, E^T)\mathrm{d}E^T \,,$$

(6)

where T is the live time of the detector, and A^{eff} its effective area obtained from [7], in which A^{eff} has been averaged over neutrinos and anti-neutrinos. $R(x^R, x^T)$ is a resolution function, which is responsible for the smearing between the reconstructed and true parameters x^R and x^T, respectively. We assume a log-normal distribution, giving it the form

$$R(x^R, x^T) = \frac{1}{\sqrt{2\pi}\sigma_{x^R} x^R} \exp\left[-\frac{(\log x^R - \mu(x^T))^2}{2\sigma_{x^R}^2}\right] \,.$$

(7)

However, the energy reconstruction is biased, meaning that the most probable reconstructed energy for a given true energy is not the same due to systematic differences [8]. Thus, we don't assume that $\mu(E^T) = E^R$. To model this relationship between E^T and E^R, we fit a Gaussian process regressor on the IC-86 Monte Carlo dataset from [9], from which we can extract a predicted mean and standard deviation for a given E^R. We then take the E^T points of the 99th percentile of each reconstructed distribution to obtain the E^T limits over which to integrate. We take the angular resolution function to be identically unity since the angle resolution in IceCube for track-like events is less than 2°, making $\cos(\theta_z^T)$ practically coincide with $\cos(\theta_z^R)$ for our study [6].

B. DeepCore

We use the publically available DeepCore data sample [10] which is an updated version of what was used by the IceCube collaboration in a ν_μ disapprearance analysis [11].

The detector systematics include ice absorption and scattering, as well as overall, lateral, and head-on optical efficiencies of the DOMs. They are applied as correction factors using the best-fit points from the DeepCore 2019 ν_τ appearance analysis [12].

The data include 14901 track-like events and 26001 cascade-like events, both divided into eight $\log_{10} E^R \in [0.75, 1.75]$ bins (index i), eight $\cos(\theta_z^R) \in [-1, 1]$ bins (index j), and two bins for the event classification (index k). Each event has a Monte Carlo weight $w_{ijk,\beta}$ from which we can construct the event count as

$$N_{ijk} = C_{ijk} \sum_\beta w_{ijk,\beta}\, \phi_\beta^{\mathrm{det}}\,, \tag{8}$$

where C_{ijk} is the correction factor from the detector systematic uncertainty and $\phi_\beta^{\mathrm{det}}$ is defined as Eq. 5. We have now substituted the effect of the Gaussian smearing by treating the reconstructed and true quantities as a migration matrix.

C. PINGU

The methodology behind the PINGU simulations is the same as with our DeepCore study II B. We use the public Monte Carlo [13], which allows us to construct the event count as in Eq. 8. However, since no detector systematics is yet modeled for PINGU, we take the correction factors C_{ijk} are all unity. We will remedy this by including an uncorrelated systematic error, which we can scale at will. As with the DeepCore Monte Carlo, the PINGU Monte Carlo is divided into eight $\log_{10} E^R \in [0.75, 1.75]$ bins, and eight $\cos(\theta_z^R) \in [-1, 1]$ bins for both track- and cascade-like events. We plot the normalized event differences $(N_{NSI} - N_{SI})/\sqrt{N_{SI}}$ for cascades and tracks in Fig. 6. We generate 'data' by predicting the event rates at PINGU with the following best-fit parameters from [14], except for the CP-violating phase which is set to zero for simplicity.

$$\Delta m_{21}^2 = 7.42 \times 10^{-5}\,\mathrm{eV}^2,\ \ \Delta m_{31}^2 = 2.517 \times 10^{-3}\,\mathrm{eV}^2,$$
$$\theta_{12} = 33.44°, \quad \theta_{13} = 8.57°, \quad \theta_{23} = 49.2°, \quad \delta_{\mathrm{CP}} = 0\,. \tag{9}$$

III. RESULTS

At the reconstructed event level, we note that the $\epsilon_{\mu\tau}$ features discussed in Sec. I B display themselves differently in each detector. We investigate this for $\epsilon_{\mu\tau}$ by in Fig. 3a plotting the muon survival probability difference $P_{\mu\mu}(\epsilon_{\mu\tau}^+) - P_{\mu\mu}(\epsilon_{\mu\tau}^-)$, where $\epsilon_{\mu\tau}^\pm = \pm 0.01$. Comparing Fig. 3a with the flux ratios in Fig. 3b, we see that the reconstruction of PINGU is superior to DeepCore, since the event ratio $\log(N_{NSI}^+/N_{NSI}^-) = \log N_{NSI}^+ - \log N_{NSI}^-$ (in reconstructed quantities) more closely matches the probability difference $P^+ - P^-$ (in true quantities). This is most evident below $20\,\mathrm{GeV}$, where the DeepCore reconstruction has washed out the fringes while PINGU preserves the N_{NSI}^- surplus below $10\,\mathrm{GeV}$.

Now we turn to the effect of $\epsilon_{\mu\tau}$. Muon events are the most abundant, and it suffices to study $P_{\mu\mu}$ in this way to explain the $\epsilon_{\mu\tau}$ features. First, let $P^\pm$ denote $P_{\mu\mu}(\epsilon_{\mu\tau}^\pm)$. We see see that $\epsilon_{\mu\tau}^+$ generates a slightly higher $P_{\mu\mu}$ for energies around $20\,\mathrm{GeV}$ (blue area), while $\epsilon_{\mu\tau}^-$ produces higher $P_{\mu\mu}$ for almost all other combinations of $E^T, \cos(\theta_z^T)$. As we see in Fig. 2, this muon survival abundance is indeed preserved at flux level. So the flux for $\epsilon_{\mu\tau}^+$ is higher than the flux for $\epsilon_{\mu\tau}^-$. Is this still true at event level, i.e. after reconstruction? As we see in Fig. 3b, the binned PINGU event counts display strong differences for many bins, which will give a high statistics on both sides of $\epsilon_{\mu\tau} = 0$, slightly favoring $\epsilon_{\mu\tau}^-$. DeepCore on the other hand, has fewer bins where the event count for $\epsilon_{\mu\tau}^-$ surpasses the event count for $\epsilon_{\mu\tau}^+$, giving weaker statistics for the negative side. Thus, we conclude that we will see a $\epsilon_{\mu\tau}$ GeV-asymmetry stemming from the lower statistics for negative $\epsilon_{\mu\tau}$ at probability level, which is then propagated through the flux and finally affects the reconstruction.

(a) $P_{\mu\mu}(\epsilon_{\mu\tau}^{+}) - P_{\mu\mu}(\epsilon_{\mu\tau}^{-})$ using $\epsilon_{\mu\tau}^{\pm} = \pm 0.01$

(b) The best-fit event count ratio from each detector for $\epsilon_{\mu\tau} = \pm 0.01$. IceCube only observes a small surplus of events for $\epsilon_{\mu\tau} = -0.01$ compared to DeepCore and PINGU due to the weak NSI effect at high GeV energies.
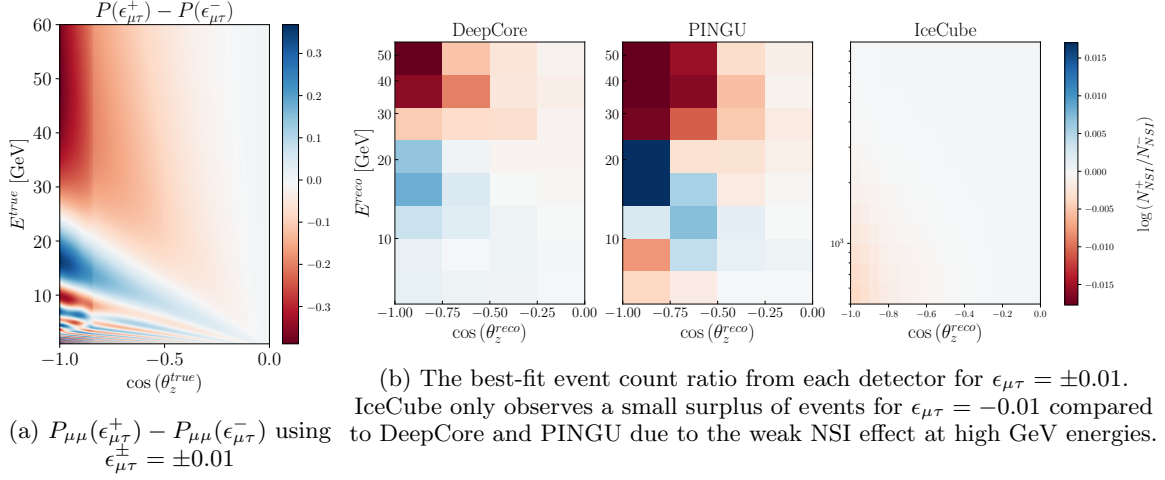
FIG. 3: Probability difference and best-fit event count. Negative $\epsilon_{\mu\tau}$ has the strongest signal, as the thin blue region stemming from $\epsilon_{\mu\tau} = 0.01$ is less prominent than the red regions from $\epsilon_{\mu\tau} = -0.01$.

A. Constraining the NSI parameters

In this section, we will constrain the four NSI parameters $\epsilon_{\tau\tau}$, $\epsilon_{\mu\tau}$, $\epsilon_{e\mu}$, and $\epsilon_{e\tau}$ by considering the detectors separately as well as jointly. For our analyses, we define our χ^2 as

$$\chi^2(\hat{\theta}, \alpha, \beta, \kappa) = \sum_{ijk} \frac{\left(N^{\text{th}} - N^{\text{data}}\right)_{ijk}^2}{\left(\sigma_{ijk}^{\text{data}}\right)^2 + \left(\sigma_{ijk}^{\text{syst}}\right)^2} + \frac{(1-\alpha)^2}{\sigma_\alpha^2} + \frac{\beta^2}{\sigma_\beta^2} \tag{10}$$

where we minimize over the model parameters $\hat{\theta} \in \{\Delta m_{31}^2, \theta_{23}, \epsilon\}$, the penalty terms α and β, and the free parameter κ. N_{ijk}^{th} is the expected number of events from theory, and N_{ijk}^{data} is the observed number of events in that bin.

In our simulations of N_{ijk}^{th}, we set all standard oscillation parameters to their current best-fit values of Eq. 9, except for Δm_{31}^2 and θ_{23} which we vary over their 3σ limits $2.435 \times 10^{-3}\,\text{eV}^2$ to $2.598 \times 10^{-3}\,\text{eV}^2$ and $40.1°$ to $51.7°$, respectively.

We set $\sigma_\alpha = 0.25$ as the atmospheric flux normalization error, and $\sigma_\beta = 0.04$ as the zenith angle slope error [3]. The observed event number has an associated Poissonian uncertainty $\sigma_{ijk}^{\text{data}} = \sqrt{N_{ijk}^{\text{data}}}$. For IceCube, the event count takes the form

$$N_{ij}^{\text{th}} = \alpha \left[1 + \beta(0.5 + \cos(\theta_z^R)_i)\right] N_{ij}(\hat{\theta}), \tag{11}$$

with $N_{ij}(\hat{\theta})$ from Eq. 6. Here, we allow the event distribution to rotate around the median cosine-zenith of $\cos(\theta_z^R) = -0.5$.

For DeepCore and PINGU, and the event count takes the form

$$N_{ijk}^{\text{th}} = \alpha \left[1 + \beta \cos(\theta_z^R)_i\right] N_{ijk}(\hat{\theta}) + \kappa N_{ijk}^{\mu_{atm}}, \tag{12}$$

with $N_{ijk}(\hat{\theta})$ from Eq. 8. $N_{ijk}^{\mu_{atm}}$ is the muon background, which is left to float freely in the DeepCore analysis. The background at PINGU can be considered negligible to first order [13], and we thus put $\kappa = 0$ when calculating the PINGU χ^2. For DeepCore and PINGU, the median cosine-zenith is $\cos(\theta_z^R) = 0$, and we allow the event count to rotate around this point.

We treat the uncorrelated systematic uncertanties differently for each detector. For IceCube, we set $\sigma_{ijk}^{\text{syst}} = f\sqrt{N_{ijk}^{\text{data}}}$. We consider best, normal, and worst-case scenarios in IceCube using $f = 5\%$, 10%, and 15% respectively. For PINGU, we use the same form but instead use $f = 0\%$, 3%, and 5%. For DeepCore, we use the provided systematic error distribution which accounts for uncertainties in the finite MC statistics and the data-driven muon background estimate [10]. This is summarized in Table I.

Experiment	Best case	Baseline	Worst case
IceCube	5%	10%	15%
PINGU	0%	3%	5%

TABLE I: Our definition of the best, baseline, and worst case scenarios considered in each experiment, modelled by $\sigma_{ijk}^{\mathrm{syst}} = f\sqrt{N_{ijk}^{\mathrm{data}}}$ with f from the table. We do not consider different DeepCore scenarios because her systematic error distribution is already provided in the data release [10].
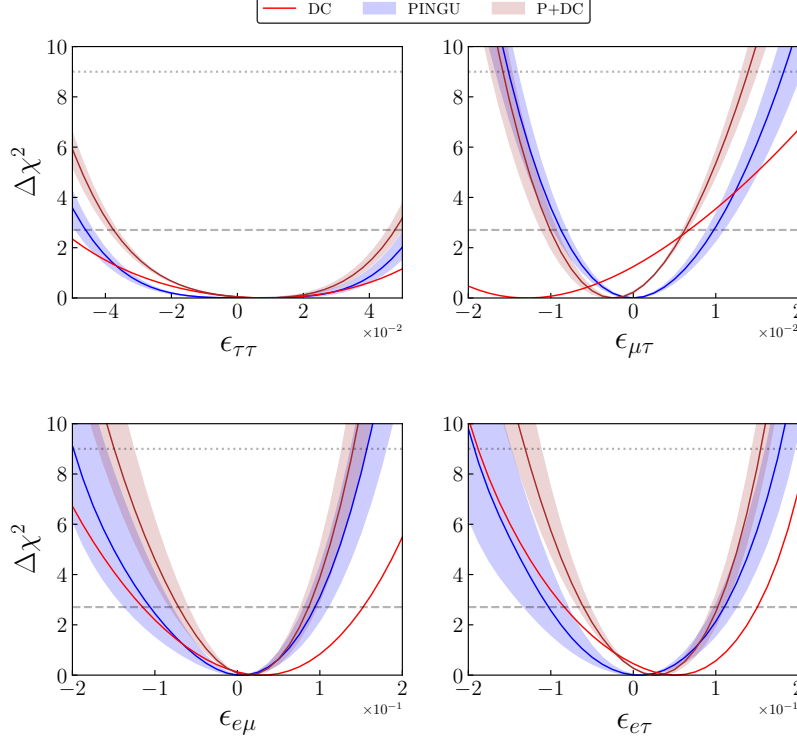

FIG. 4: PINGU and DeepCore best-case scenario, with their joint $\Delta\chi^2$ in black. Δm_{31}^2 and θ_{23} and have been marginalized out, and all other NSI parameters not shown in each panel are fixed to zero. IceCube tracks only reveal $\epsilon_{\mu\tau}$, and are displayed separately in Fig. 5.

For the joint analysis, we follow the parameter goodness-of-fit prescription [15] and construct the joint χ^2 as

$$\chi_{\mathrm{joint}}^2 = \sum_{\mathrm{exp}} \chi_{\mathrm{exp}}^2 - \chi_{\mathrm{exp,min}}^2 \tag{13}$$

with test statistic $\chi_{\mathrm{joint,min}}^2$. The $\Delta\chi_{\mathrm{joint}}^2$ is then $\Delta\chi_{\mathrm{joint}}^2 = \chi_{\mathrm{joint}}^2 - \chi_{\mathrm{joint,min}}^2$.

After the oscillation parameters have been marginalized out, we plot $\Delta\chi^2$ for each of the four NSI parameters in Fig. 4. The results are shown in Fig. 5 and summarized in Tables II and III.

Comparing the PINGU and the DeepCore results in Fig. 4, we note that the best-fit for each NSI parameter for the PINGU experiment is expected to be zero. This is because the 'data' we generated during the PINGU simulations assume no NSI since they have yet to be observed in nature. This introduces a non-NSI bias in all joint analyses which include PINGU, since PINGU has stronger statistics than DeepCore and will thus pull the joint χ^2 towards $\epsilon = 0$.
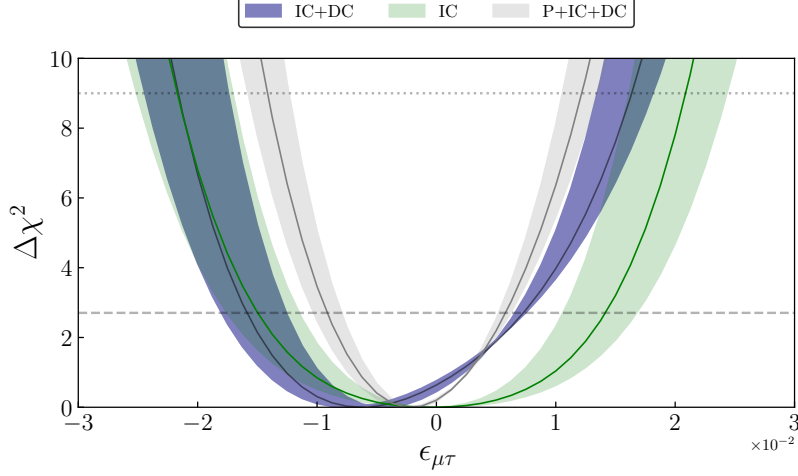
FIG. 5: $\epsilon_{\mu\tau}$ $\Delta\chi^2$ regions for scenarios as defined in Table I. Δm_{31}^2 and θ_{23} and have been marginalized out, and all other NSI parameters other than $\epsilon_{\mu\tau}$ are fixed to zero.

Parameter	Best 90% CL	Best 3σ	Baseline 90% CL	Baseline 3σ	Worst 90% CL	Worst 3σ
			IceCube			
$\epsilon_{\mu\tau}$	[-0.008, 0.009]	[-0.014, 0.017]	[-0.009, 0.01]	[-0.015, 0.018]	[-0.01, 0.011]	[-0.017, 0.02]
			DeepCore			
$\epsilon_{\tau\tau}$	[-0.044, 0.051]	[-0.062, 0.069]	[-0.046, 0.054]	[-0.065]	[-0.049, 0.057]	[-0.07]
$\epsilon_{\mu\tau}$	[-0.008, 0.009]	[-0.014, 0.017]	[-0.009, 0.01]	[-0.015, 0.018]	[-0.01, 0.011]	[-0.017, 0.02]
$\epsilon_{e\mu}$	[-0.079, 0.081]	[-0.16, 0.14]	[-0.11, 0.094]	[-0.20, 0.16]	[-0.14, 0.11]	[-0.23, 0.18]
$\epsilon_{e\tau}$	[-0.079, 0.098]	[-0.15, 0.16]	[-0.10, 0.11]	[-0.19, 0.18]	[-0.13, 0.13]	[-0.23, 0.12]
			IceCube + DeepCore			
$\epsilon_{\mu\tau}$	[-0.029, 0.007]	[0.026]	[-0.029, 0.007]	[0.026]	[-0.029, 0.007]	[0.026]

TABLE II: IceCube and DeepCore results from the $\Delta\chi^2$ in Fig. 5. Best, baseline, and worst refer to the systematic uncertainty scenarios considered as in Table I.

[1] Search for Nonstandard Neutrino Interactions with IceCube DeepCore - INSPIRE.
URL https://inspirehep.net/literature/1624684
[2] A. M. Dziewonski and D. L. Anderson, Preliminary reference Earth model 25 (4) 297–356. doi:10.1016/0031-9201(81)90046-7.
[3] M. Honda et al., Calculation of atmospheric neutrino flux using the interaction model calibrated with atmospheric muon data.doi:10.1103/PhysRevD.75.043006.
[4] I. Collaboration et al., All-flavor constraints on nonstandard neutrino interactions and generalized matter potential with three years of IceCube DeepCore data. arXiv:2106.07755.
URL http://arxiv.org/abs/2106.07755
[5] T. I.-P. Collaboration, Letter of Intent: The Precision IceCube Next Generation Upgrade (PINGU). arXiv:1401.2046.
URL http://arxiv.org/abs/1401.2046
[6] M. G. Aartsen et al., Searching for eV-scale sterile neutrinos with eight years of atmospheric neutrinos at the IceCube Neutrino Telescope 102 (5) 052009. doi:10.1103/PhysRevD.102.052009.
[7] IceCube Collaboration, All-sky point-source IceCube data: Years 2010-2012. doi:10.21234/B4F04V.
[8] C. Weaver, Evidence for Astrophysical Muon Neutrinos from the Northern Sky 149.

Parameter	Best 90% CL	Best 3σ	Baseline 90% CL	Baseline 3σ	Worst 90% CL	Worst 3σ
			PINGU			
$\epsilon_{\tau\tau}$	[-0.054, 0.067]	[]	[-0.054, 0.067]	[]	[-0.054, 0.067]	[]
$\epsilon_{\mu\tau}$	[-0.029, 0.007]	[0.026]	[-0.029, 0.007]	[0.026]	[-0.029, 0.007]	[0.026]
$\epsilon_{e\mu}$	[-0.12, 0.15]	[-0.23, 0.24]	[-0.12, 0.15]	[-0.23, 0.24]	[-0.12, 0.15]	[-0.23, 0.24]
$\epsilon_{e\tau}$	[-0.084, 0.15]	[-0.19, 0.21]	[-0.084, 0.15]	[-0.19, 0.21]	[-0.084, 0.15]	[-0.19, 0.21]
			DeepCore + PINGU			
$\epsilon_{\tau\tau}$	[-0.036, 0.046]	[-0.056, 0.064]	[-0.038, 0.048]	[-0.058, 0.067]	[-0.039, 0.05]	[-0.06]
$\epsilon_{\mu\tau}$	[-0.009, 0.006]	[-0.015, 0.013]	[-0.01, 0.006]	[-0.016, 0.014]	[-0.011, 0.007]	[-0.017, 0.015]
$\epsilon_{e\mu}$	[-0.06, 0.077]	[-0.126, 0.127]	[-0.071, 0.086]	[-0.149, 0.141]	[-0.082, 0.097]	[-0.17, 0.16]
$\epsilon_{e\tau}$	[-0.052, 0.095]	[-0.112, 0.144]	[-0.061, 0.103]	[-0.131, 0.155]	[-0.067, 0.11]	[-0.15, 0.17]
			IceCube + DeepCore + PINGU			
$\epsilon_{\mu\tau}$	[-0.009, 0.006]	[-0.015, 0.013]	[-0.01, 0.006]	[-0.016, 0.014]	[-0.011, 0.007]	[-0.017, 0.015]

TABLE III: PINGU and joint results from the $\Delta\chi^2$ in Fig. 4. Best, baseline, and worst refer to the systematic uncertainty scenarios considered as in Table I.

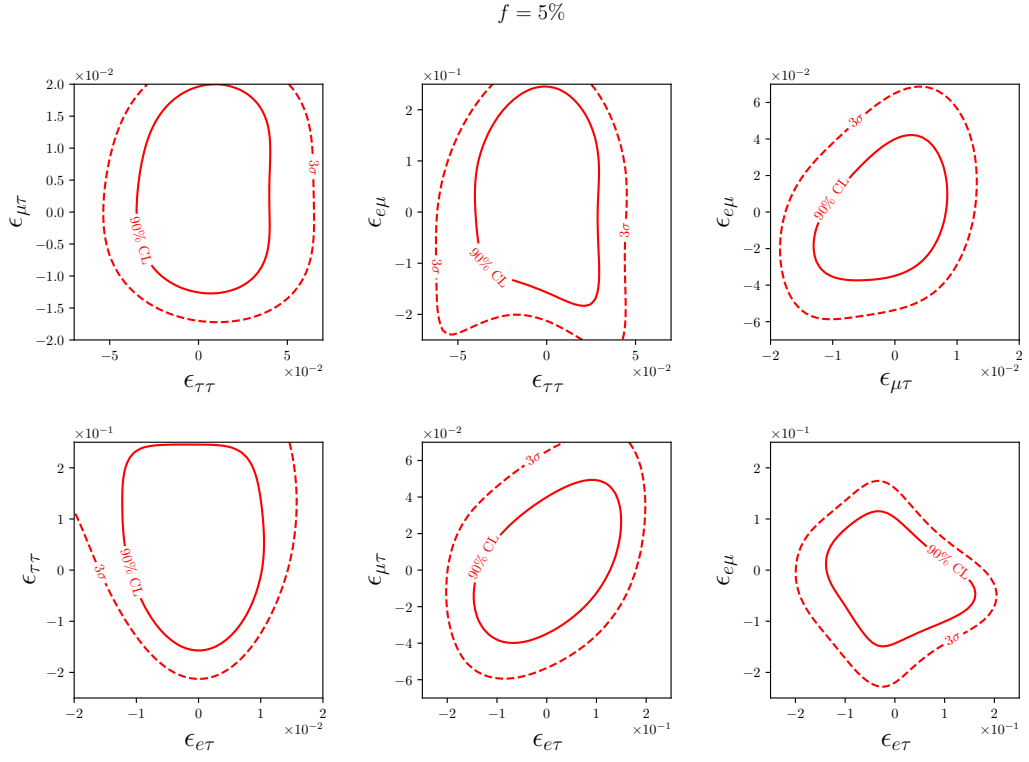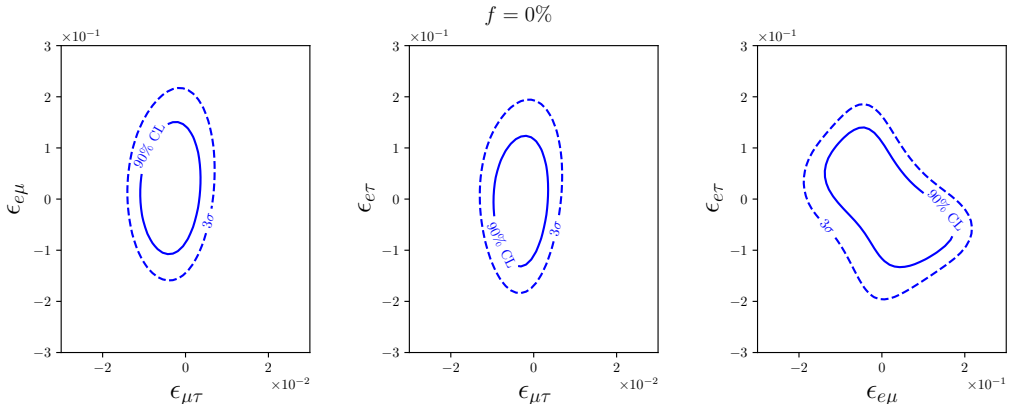|	Best fit		
Parameter	Δm_{31}^2	θ_{23}	ϵ
	DeepCore		
$\epsilon_{\tau\tau}$	2.435	47.84	0.0125
$\epsilon_{\mu\tau}$	2.435	43.97	-0.005
$\epsilon_{e\mu}$	2.435	43.97	0
$\epsilon_{e\tau}$	2.435	43.97	0.05
	IceCube		
$\epsilon_{\mu\tau}$	2.435	51.70	0
	IceCube + DeepCore		
$\epsilon_{\mu\tau}$	2.517	43.97	-0.01

TABLE IV: Best fit points for Δm_{31}^2 and θ_{23} are given in units of 10^{-3}eV^2 and degrees, respectively.

[9] IceCube Collaboration, Search for sterile neutrinos with one year of IceCube data. URL https://icecube.wisc.edu/data-releases/2016/06/search-for-sterile-neutrinos-with-one-year-of-icecube-data/

[10] IceCube Collaboration, Three-year high-statistics neutrino oscillation samples. doi:10.21234/ac23-ra43.

[11] IceCube Collaboration et al., Measurement of Atmospheric Neutrino Oscillations at 6–56 GeV with IceCube DeepCore 120 (7) 071801. doi:10.1103/PhysRevLett.120.071801.

[12] IceCube Collaboration 1 et al., Measurement of atmospheric tau neutrino appearance with IceCube DeepCore 99 (3) 032007. doi:10.1103/PhysRevD.99.032007.

[13] IceCube Collaboration, IceCube Upgrade Neutrino Monte Carlo Simulation. doi:10.21234/qfz1-yh02.

[14] I. Esteban et al., The fate of hints: Updated global analysis of three-flavor neutrino oscillations 2020 (9) 178. doi:10.1007/JHEP09(2020)178.

[15] M. Maltoni and T. Schwetz, Testing the statistical compatibility of independent data sets 68 (3) 033020. arXiv:hep-ph/0304176, doi:10.1103/PhysRevD.68.033020.
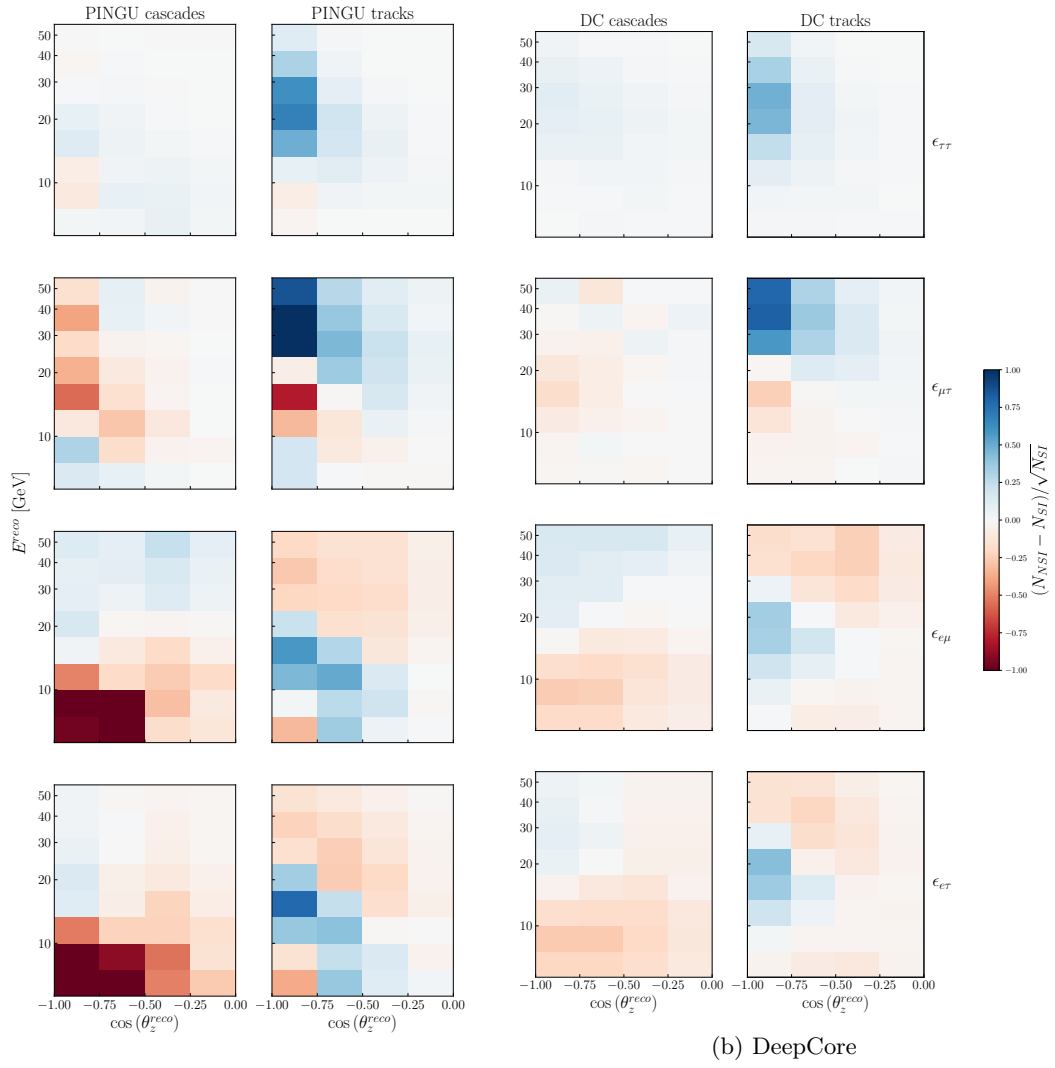
(a) PINGU

(b) DeepCore

FIG. 6: Expected pulls of the form $(N_{NSI} - N_{SI})/\sqrt{N_{SI}}$ for PINGU and DeepCore after 3 years.

$f = 0\%$

$f = 5\%$

DeepCore (2017)

- ✓ Honda atmospheric fluxes
- × Only look at tracks and $\epsilon_{\mu\tau}$
- × DC Monte Carlo from an older dataset
- × 8 E bins from $6.3\,\mathrm{eV}^2$ to $56\,\mathrm{eV}^2$
- × 8 z bins from -1 to 0
- × Use "Overall" and "relative ν_e to ν_μ" normalization
- × Prior on spectral index
- × No zenith angle normalization
- ✓ No priors on $\Delta m^2_{31}, \theta_{23}, \theta_{13}$

Demidov (2020) DC analysis

- ✓ Honda atmospheric fluxes
- ✓ Looks at tracks + cascades for $\epsilon_{\mu\tau}$ and $\epsilon_{\tau\tau}$
- ✓ Data and Monte Carlo from DC 2018
- ✓ 8 E bins from $5.6\,\mathrm{eV}^2$ to $56\,\mathrm{eV}^2$
- ✓ 8 z bins from -1 to 1
- × Use "Overall" and "relative ν_e to ν_μ" normalization
- × Prior on spectral index
- × No zenith angle normalization
- ✓ No priors on $\Delta m^2_{31}, \theta_{23}$
- ✓ Fixes $\Delta m^2_{21}, \theta_{12}, \theta_{13}$
- × Uncertainty on hadron production in atmosphere
- × Uncertainty on neutrino nucleon cross section

This DC+PINGU analysis

- ✓ Honda atmospheric fluxes
- ✓ Tracks and cascades for all flavors
- ✓ Reco → true mapping from Monte Carlo migration matrix
- ✓ 8 E bins from $5.6\,\mathrm{eV}^2$ to $56\,\mathrm{eV}^2$
- ✓ 8 zenith angle bins from -1 to 1
- ✓ Flux normalization uncertainty of 25%
- ✓ Zenith angle uncertainty of 4%
- ✓ No priors on oscillation parameters
- ✓ Marginalize Δm^2_{31} and θ_{23}. All other oscillation parameters are fixed.